A Two-Step Approach for the Analysis of Bulk Current Injection Setups Involving Multiwire Bundles

Nicola Toscani , *Member, IEEE*, Xinglong Wu , *Member, IEEE*, Domenico Spina , *Member, IEEE*, Dries Vande Ginste , *Senior Member, IEEE*, and Flavia Grassi , *Senior Member, IEEE*

Abstract—In this work, a two-step procedure to predict maximum (worst-case scenario) and minimum (best-case scenario) noise levels induced by bulk current injection (BCI) at the terminal sections of a wiring harness is presented. To this end, common mode (CM) and differential mode (DM) quantities are introduced by a suitable modal transformation, and equivalent modal circuits are derived, where CM (dominant mode) into DM (secondary mode) conversion is modelled by induced sources included into the DM circuit. The procedure initially foresees the solution of the CM circuit to provide input data for subsequent solution of the DM circuit. Such a two-step approach is then used to develop a probabilistic–possibilistic framework for computationally-efficient estimation of lower and upper boundaries to the variability of the noise voltages induced at the bundle terminations. To this end, random uncertainty affecting certain setup parameters is addressed through probability theory, whereas epistemic uncertainty is represented via possibility theory. Accuracy and computational efficiency of the proposed two-step method are assessed by examples involving seven and nineteen wire harnesses.

Index Terms—Bulk current injection (BCI), conducted susceptibility, epistemic uncertainty, hybrid probabilistic–possibilistic uncertainty quantification, modal analysis, multiconductor transmission lines.

I. Introduction

BULK current injection (BCI) is widely recognized to be a simple but effective technique for conducted susceptibility assessment of electrical/electronic systems. As a matter of fact, BCI-based procedures are foreseen by several electromagnetic compatibility (EMC) standards for aerospace [1], automotive [2], industrial [3], and military [4] applications. Furthermore, it has been shown in the literature that BCI setups can be also exploited to reproduce the noise induced in the terminal units by traditional radiated susceptibility (RS) effects [5] and electromagnetic pulse tests [6]. For these reasons,

modeling of BCI probes and test setups has gained increasing attention from the EMC community. Consequently, several modeling techniques have been developed over the years, including analytical models [7], circuit models suitable for SPICE-based simulations [8], [9], [10], and behavioral models [11], [12].

Most of the aforesaid models deal with simple wiring structures only (e.g., two or three-wire interconnections [13]), whereas BCI setups often involve cable harnesses [2], [14]. In this case, the actual noise injected into the terminal units can be significantly affected by the specific arrangement of the cable [14], [15]. Hence, accurate modeling is not only of the injection device but also of the wiring structure is required in order to achieve accurate prediction of the actual noise injected in the terminal units. An example is the model proposed in [15], where the dependence of the induced noise on geometrical characteristics of the wiring harness was investigated. However, the analysis in [15] was carried out in terms of physical voltages/currents only. Hence, it does not allow to easily appreciate the geometrical/electrical parameters influencing the propagation of the injected currents. As a matter of fact, if the probe is clamped on a multiwire harness, a bulk common-mode (CM) current is injected in all wires, and the noise induced at terminals is expected to be the same if the impedance to ground of all wires is the same. The observed differences, however, are due to the presence of nonnull differential modes (DMs), which are to be ascribed to asymmetries with respect to ground of the wires in the bundle, as well as to possible differences in the terminal sections. To thoroughly investigate these effects, this work reformulates the problem in terms of modal quantities, and proposes a computationally efficient two-step approach to provide boundaries to the variability of CM and DM noise quantities due to uncertainties affecting geometrical/electrical parameters of the BCI setup.

To achieve this result, the first step is to leverage on modal analysis to evaluate accurate deterministic modal circuits of BCI setups involving wiring harnesses. Namely, this work considers wire bundles involving at least seven conductors. To this end, an *ad hoc* modal transformation matrix is introduced, through which one CM and $(N-1)$ DMs can be defined for any arbitrary number of wires N. In literature several modal circuits are available [16], [17], also including mode conversion [18], [19], [20], however, these models are applicable to a limited number of wires (most of them dealing with wiring structures for differential signaling only [21]). Therefore, those works represent the background of the present analysis, which exploits

and generalizes some of the assumptions there introduced (as for instance, the assumption of weak coupling between modal circuits) to derive simple yet accurate modal equivalent circuits of BCI setup involving wiring harnesses. First of all, since the noise injected by BCI has an inherent CM nature, the BCI probe is modeled in the CM circuit only, and the presence of nonnull DM voltages and currents is ascribed to CM into DM conversion. Also, the presence of a dominant mode (CM) is exploited to formulate the assumption of weak coupling between the CM and the other DM circuits, with the advantage to neglect the reconversion of the induced DMs (secondary modes) into CM (primary mode), i.e., the so-called *back interaction* in [22]. Conversely, all couplings/interactions among the DM modes are retained and properly modeled.

The aforesaid deterministic model clearly unveils the mechanism of CM into DMs conversion in BCI setups, and can be effectively used to speed up the statistical analysis of BCI setups whose geometrical/electrical parameters are affected by uncertainty or are not completely known to the operator. As a matter of fact, preliminary simulations revealed that variability of these parameters does not equally influence both CM and DM quantities, thus suggesting the possibility to organize the solution into two steps not only for deterministic, but also for statistical investigations.

More specifically, in this work such a two-step approach is developed to identify the maximum (worst-case scenario) and minimum (best-case scenario) noise levels, that can be expected at the terminations of the bundle under analysis due to uncertainty affecting geometrical/electrical parameters. With respect to traditional statistical investigations, where uncertain parameters are usually modeled as random variables (RVs) and assigned specific probability distribution functions, here it is recognized that the values of some parameters are actually uncertain not due to stochastic variability, but because they are not known *a priori* to the operator and cannot be measured (so called epistemic uncertainty [23]). Hence, these parameters are modeled as possibilistic instead of probabilistic variables, and assigned suitable possibility distributions. More specifically, geometrical and electrical parameters describing the wiring harness are treated as traditional RVs assigned with Gaussian probability distribution functions around their nominal values [24], [25], [26]. Conversely, the CM equivalent impedance to ground, whose value is usually unknown to the operator unless preliminary measurements on the actual test setup can be run, is modeled as a possibilistic variable, assigned with a uniform possibility distribution, which better represents the actual lack of information affecting the knowledge of this parameter [23].

To sum up, with respect to traditional models, the proposed two-step procedure has the following advantages: first, it provides independent distributed-parameter CM and DM equivalent circuits of the whole setup. Second, thanks to this approach, geometrical and electrical parameters mostly affecting the CM and DM noise injected at terminations can be easily identified. Third, since the coupling mechanism between the probe and a multiwire bundle mainly involves the CM, the proposed CM equivalent circuit can retain the majority of information about the injected noise. Finally, to properly deal with
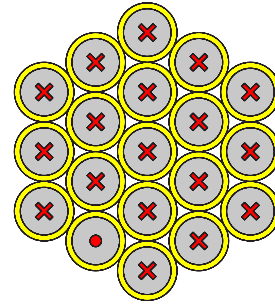

Fig. 1. Reference cross section of a 19-wire bundle together with the definition of a generic DM. Configurations involving 7 and 13 conductors can be obtained by removing the outer wires. The red crosses mean currents entering the conductors, whereas the red dot means current going out from the wire. These two symbols explain how a generic DM is defined.
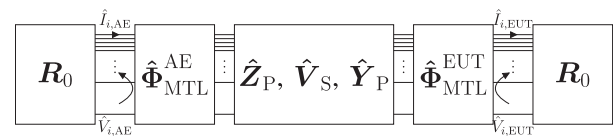

Fig. 2. Chain-parameter (Block) representation of the equivalent MTL circuit of a N-wire BCI-based test setup. The scheme highlights the equipment under test (EUT) and the auxiliary equipment (AE) sides [15].

uncertainties in BCI setups, a probabilistic–possibilistic framework involving the two-step procedure is developed. As a result, the N-conductor problem can be split into two subproblems, whose solution is more efficient than the solution of the original problem [15], thus, providing reliable worst and best-case noise predictions.

The article is organized as follows. Section II introduces the proposed deterministic model, whose accuracy in the prediction of modal and physical voltages/currents is then investigated in Section III. Probabilistic and possibilistic variables are introduced and assigned suitable distributions in Section IV, where the proposed two-step approach is used to evaluate maximum and minimum noise levels induced at terminations of the wiring harness during the test, proving the accuracy and computational efficiency of the proposed method. Conclusions are drawn in Section V.

II. TWO-STEP MODELING APPROACH IN THE MODAL DOMAIN

In previous work [15], a circuit representation of a setup involving a BCI probe clamped on N-wire multiconductor transmission lines (MTLs) was developed. The model allows the prediction of phase voltages at terminations of canonical setups, i.e., 7, 13, and 19 conductors arranged similarly to the cross-section reported in Fig. 1 and terminated with $R_0 = 50\,\Omega$ resistors were considered. To this end, the setup was modeled as the cascaded connection of chain-parameter matrices (see Fig. 2) and solved for the physical voltages and currents. Possible differences in terms of voltage levels computed at terminations can then be observed owing to interactions between each wire and the probe, the ground plane and the other victim conductors. In this work, the behavior of BCI probes clamped on N-wire

bundles is studied via a modal decomposition instead, given the motivations presented in Section I. In particular, the system under study is analyzed considering one CM and $N-1$ DMs.

A. Definition of Modal Quantities

The canonical definition of modal quantities for two-conductor systems [27], [28] is here extended to the case of an N-wire harness. To this end, the following modal transformation matrices are proposed and used in this work:

$$
\boldsymbol{T}_V = \begin{bmatrix}
1 & 1/N & \cdots & \cdots & \cdots & 1/N \\
1 & -1/N & 0 & \cdots & \cdots & 0 \\
1 & 0 & -1/N & 0 & \cdots & 0 \\
\vdots & \vdots & \ddots & \ddots & \ddots & \vdots \\
1 & 0 & \cdots & 0 & -1/N & 0 \\
1 & 0 & \cdots & \cdots & 0 & -1/N
\end{bmatrix} \tag{1}
$$

$$
\boldsymbol{T}_I = \begin{bmatrix}
1/N & 1 & \cdots & \cdots & \cdots & 1 \\
1/N & -1 & 0 & \cdots & \cdots & 0 \\
1/N & 0 & -1 & 0 & \cdots & 0 \\
\vdots & \vdots & \ddots & \ddots & \ddots & \vdots \\
1/N & 0 & \cdots & 0 & -1 & 0 \\
1/N & 0 & \cdots & \cdots & 0 & -1
\end{bmatrix}. \tag{2}
$$

The vectors of modal voltages $\hat{\boldsymbol{V}}_m$ and currents $\hat{\boldsymbol{I}}_m$ can be obtained from the line voltages $\hat{\boldsymbol{V}}$ and currents $\hat{\boldsymbol{I}}$ as follows:

$$
\hat{\boldsymbol{V}}_m = \begin{bmatrix} \hat{V}_{\text{CM}} \\ \hat{V}_{\text{DM1}} \\ \vdots \\ \hat{V}_{\text{DM}(N-1)} \end{bmatrix} = \boldsymbol{T}_V^{-1} \hat{\boldsymbol{V}} \tag{3}
$$

$$
\hat{\boldsymbol{I}}_m = \begin{bmatrix} \hat{I}_{\text{CM}} \\ \hat{I}_{\text{DM1}} \\ \vdots \\ \hat{I}_{\text{DM}(N-1)} \end{bmatrix} = \boldsymbol{T}_I^{-1} \hat{\boldsymbol{I}}. \tag{4}
$$

Accordingly, CM quantities appear at the top of each modal vector, and the $N-1$ DMs are defined as shown in Fig. 1. Namely, a current is injected in one of the conductors different from the one placed at the center of the bundle, and it returns in all the other wires. The definition of such DMs does not involve any orthonormal transformation. Hence, the matrices we will obtain by applying these transformations are not diagonal.

B. Modal Equivalent Circuits

Although the noise injected by clamping the probe on the harness has a CM nature, the DM noise induced at the terminal units is usually not null. This is due to undesired CM-to-DM conversions introduced by possible unbalance affecting the terminal units and interactions between wires in the structures of the MTL

running outside the BCI probe. In this work, the focus is mainly on the effects owing to the cable, and the mode conversion occurring along its length. Moreover, to provide an effective, yet computationally efficient, representation of the CM-to-DM conversion along the wiring harness, we will formulate and exploit the assumption of weak-coupling between the CM (dominant mode) and the $(N-1)$ DM modes previously introduced. More specifically, in analogy with crosstalk [22], [28], we will model CM-to-DM conversion by neglecting the backconversion from the induced DM to CM, since it is usually negligible with respect to the CM injected by the probe. To implement this assumption, specific entries (i.e., off-diagonal entries in the first row) of the modal per-unit-length (p.u.l.) inductance $\boldsymbol{L}_m$ and capacitance $\boldsymbol{C}_m$ matrices are zeroed. Considering a 7-conductor MTL as an example, the modal p.u.l. inductance matrix $\boldsymbol{L}_m$ is simplified as

$$
\boldsymbol{L}_m = \begin{bmatrix}
l_{\text{CM}} & 0 & \cdots & \cdots & \cdots & 0 \\
l_{1-\text{CM}} & l_1 & l_{1-2} & \cdots & \cdots & l_{1-6} \\
l_{2-\text{CM}} & l_{2-1} & l_2 & l_{2-3} & \cdots & l_{2-6} \\
\vdots & \vdots & \ddots & \ddots & \ddots & \vdots \\
l_{5-\text{CM}} & l_{5-1} & \cdots & l_{5-4} & l_5 & l_{5-6} \\
l_{6-\text{CM}} & l_{6-1} & \cdots & \cdots & l_{6-5} & l_6
\end{bmatrix} \tag{5}
$$

where l_{CM} is the CM self-inductance, $l_{i-\text{CM}}$ is the mutual inductance coupling the CM with the ith DM, l_i is the ith self-inductance, and $l_{i,j}$ is the mutual inductance coupling the ith with the jth DMs. The capacitance matrix has a similar structure. In the matrices $\boldsymbol{Y}_p$ and $\boldsymbol{Z}_p$ (i.e., the matrix coupling the probe to the wiring harness), also the entries in the first row are zeroed. This is a consequence of the CM nature of noise injection by BCI. Namely, it is assumed that the probe itself does not generate any DM disturbance, which are only due to MTL effects as previously mentioned. Based on this simplification, modal terminal voltages can be predicted in two steps. Indeed, the weak coupling assumption mentioned before allows one to solve the CM circuit first, independently of all the other DMs. A simplified equivalent circuit for the CM can be drawn as shown in Fig. 3(a). Given that, in the proposed modal decomposition approach, only one CM can be identified independently of the specific setup considered, this representation involves one conductor running above ground only. This circuit includes the radio frequency (RF) voltage source accounting for current injection on the bundle as well as equivalent CM elements associated with the injection setup. In particular, matrices $\hat{\boldsymbol{\Phi}}_{\text{fix}}^{\text{CM}}$ and $\hat{\boldsymbol{\Phi}}_{\text{TL}}^{\text{CM}}$ are 2×2 matrices, whereas the other passive elements $R_{\text{AE,EUT}}^{\text{CM}}$, $\hat{Y}_{\text{P}}^{\text{CM}}$, $\hat{Z}_{\text{P}}^{\text{CM}}$, $\hat{V}_{\text{S}}$, and R_0^{CM} are frequency-dependent scalar parameters. No coupling terms with any DM circuits need to be included as a consequence of the weak-coupling assumption. The second step is the solution of the equivalent DM circuit, which involves the $(N-1)$ modes as shown in Fig. 3(b). Vectors of controlled sources appear in this equivalent representation to account for CM-to-DMs conversion. Indeed, once a solution is available for the CM, two pairs of voltages and currents computed at the left/right side of the BCI probe (see $\hat{V}_{\text{L,R}}^{\text{CM}}$ and $\hat{I}_{\text{L,R}}^{\text{CM}}$ in Fig. 3(a)) are used to compute the entries of the vector of controlled
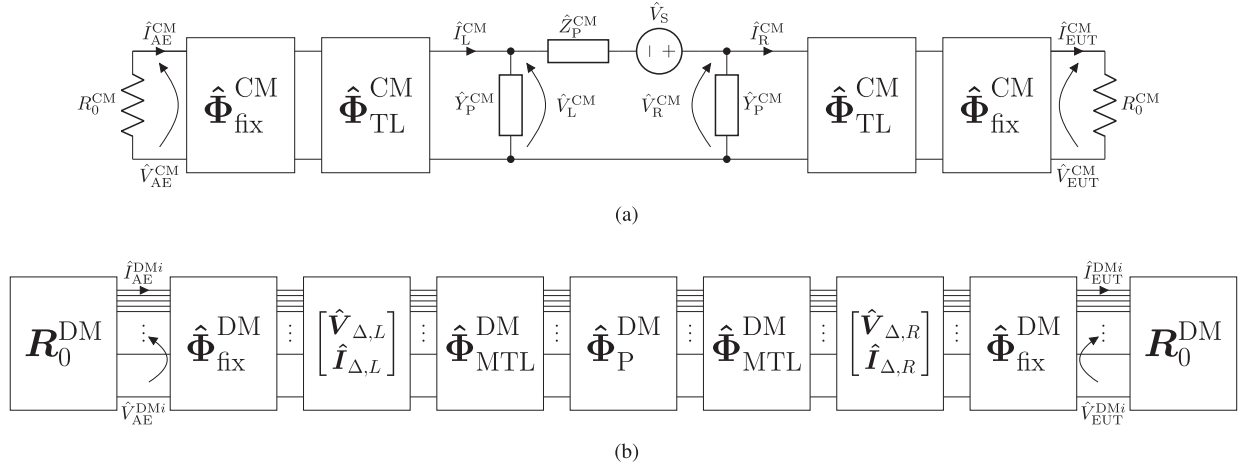
(a)

(b)

Fig. 3. Equivalent modal circuits of the BCI setup: (a) CM; (b) DM ($N - 1$ modes).

generators $\hat{\boldsymbol{V}}_\Delta$ and $\hat{\boldsymbol{I}}_\Delta$. These $2(N-1)$ sources, exciting all the DMs, are defined as

$$\begin{bmatrix} \hat{\boldsymbol{V}}_{\Delta,\mathrm{R}} \\ \hat{\boldsymbol{I}}_{\Delta,\mathrm{R}} \end{bmatrix} = \int_0^{\mathscr{L}_\mathrm{R}} \hat{\boldsymbol{\Phi}}_{\mathrm{MTL}}^{\mathrm{DM}}(\mathscr{L}_\mathrm{R} - \tau) \begin{bmatrix} -j\omega\boldsymbol{\Delta l}\hat{I}_\mathrm{R}^{\mathrm{CM}}(\tau) \\ -j\omega\boldsymbol{\Delta c}\hat{V}_\mathrm{R}^{\mathrm{CM}}(\tau) \end{bmatrix} d\tau \tag{6}$$

$$\begin{bmatrix} \hat{\boldsymbol{V}}_{\Delta,\mathrm{L}} \\ \hat{\boldsymbol{I}}_{\Delta,\mathrm{L}} \end{bmatrix} = \int_0^{\mathscr{L}_\mathrm{L}} \hat{\boldsymbol{\Phi}}_{\mathrm{MTL}}^{\mathrm{DM}}(\mathscr{L}_\mathrm{L} - \tau) \begin{bmatrix} j\omega\boldsymbol{\Delta l}\hat{I}_\mathrm{L}^{\mathrm{CM}}(\tau) \\ -j\omega\boldsymbol{\Delta c}\hat{V}_\mathrm{L}^{\mathrm{CM}}(\tau) \end{bmatrix} d\tau \tag{7}$$

where the subscripts L and R denote the left and right side of the BCI probe, respectively, $\mathscr{L}$ and $\hat{\boldsymbol{\Phi}}_{\mathrm{MTL}}$ are the length and the chain parameter matrix of the considered stretch of MTL, respectively, $\boldsymbol{\Delta c}$ and $\boldsymbol{\Delta l}$ are the first column vectors of coupling terms in the modal p.u.l capacitance and inductance matrices, respectively (i.e., terms $l_{i-\mathrm{CM}}$ in (5)). In (6) and (7), relative coordinates are adopted to obtain a general result: the origin is placed in the center of the hole of the BCI probe.

The integrals in (6) and (7) can be solved in closed form, noting that currents and voltages at a generic position τ can be rewritten as a function of $\hat{V}_\mathrm{L}^{\mathrm{CM}}(\mathscr{L})$ and $\hat{I}_\mathrm{L}^{\mathrm{CM}}(\mathscr{L})$, i.e., the same voltages and currents computed at the end of the line. Considering a generic stretch of MTL, the integration leads to

$$\hat{\boldsymbol{V}}_\Delta = -\frac{1}{4}j\omega\left(\hat{\boldsymbol{A}} - \hat{\boldsymbol{B}}\right) \tag{8}$$

$$\hat{\boldsymbol{I}}_\Delta = -\frac{1}{4}j\omega\left(-\hat{\boldsymbol{C}} + \hat{\boldsymbol{D}}\right) \tag{9}$$

where

$$\hat{\boldsymbol{A}} = -\hat{\boldsymbol{Z}}_\mathrm{C}^{\mathrm{DM}}\boldsymbol{T}_\mathrm{I}\hat{\boldsymbol{P}}\boldsymbol{T}_\mathrm{I}^{-1}\hat{\boldsymbol{Z}}_\mathrm{C}^{\mathrm{DM}^{-1}}\boldsymbol{\Delta l} \tag{10}$$

$$\hat{\boldsymbol{B}} = \hat{\boldsymbol{Z}}_\mathrm{C}^{\mathrm{DM}}\boldsymbol{T}_\mathrm{I}\hat{\boldsymbol{Q}}\boldsymbol{T}_\mathrm{I}^{-1}\boldsymbol{\Delta c} \tag{11}$$

$$\hat{\boldsymbol{C}} = \boldsymbol{T}_\mathrm{I}\hat{\boldsymbol{R}}\boldsymbol{T}_\mathrm{I}^{-1}\hat{\boldsymbol{Z}}_\mathrm{C}^{\mathrm{DM}^{-1}}\boldsymbol{\Delta l} \tag{12}$$

$$\hat{\boldsymbol{D}} = \boldsymbol{T}_\mathrm{I}\hat{\boldsymbol{S}}\boldsymbol{T}_\mathrm{I}^{-1}\boldsymbol{\Delta c}. \tag{13}$$

$\hat{\boldsymbol{Z}}_\mathrm{C}^{\mathrm{DM}}$ is the characteristic impedance matrix of the MTL associated with the $N-1$ modes, and matrices $\hat{\boldsymbol{P}}$, $\hat{\boldsymbol{Q}}$, $\hat{\boldsymbol{R}}$, and $\hat{\boldsymbol{S}}$ take the expressions

$$\hat{\boldsymbol{P}} = e^{\hat{\boldsymbol{\gamma}}_{\mathrm{DM}}\mathscr{L}}\left(\hat{\boldsymbol{F}}_{3+}\hat{\boldsymbol{F}}_{1-} + \hat{\boldsymbol{F}}_{3-}\hat{\boldsymbol{F}}_{2-}\right)$$
$$+ e^{-\hat{\boldsymbol{\gamma}}_{\mathrm{DM}}\mathscr{L}}\left(\hat{\boldsymbol{F}}_{3+}\hat{\boldsymbol{F}}_{2+} + \hat{\boldsymbol{F}}_{3-}\hat{\boldsymbol{F}}_{1+}\right) \tag{14}$$

$$\hat{\boldsymbol{Q}} = e^{\hat{\boldsymbol{\gamma}}_{\mathrm{DM}}\mathscr{L}}\left(\hat{\boldsymbol{F}}_{4+}\hat{\boldsymbol{F}}_{1-} + \hat{\boldsymbol{F}}_{4-}\hat{\boldsymbol{F}}_{2-}\right)$$
$$- e^{-\hat{\boldsymbol{\gamma}}_{\mathrm{DM}}\mathscr{L}}\left(\hat{\boldsymbol{F}}_{4+}\hat{\boldsymbol{F}}_{2+} + \hat{\boldsymbol{F}}_{4-}\hat{\boldsymbol{F}}_{1+}\right) \tag{15}$$

$$\hat{\boldsymbol{R}} = e^{\hat{\boldsymbol{\gamma}}_{\mathrm{DM}}\mathscr{L}}\left(\hat{\boldsymbol{F}}_{3+}\hat{\boldsymbol{F}}_{1-} + \hat{\boldsymbol{F}}_{3-}\hat{\boldsymbol{F}}_{2-}\right)$$
$$- e^{-\hat{\boldsymbol{\gamma}}_{\mathrm{DM}}\mathscr{L}}\left(\hat{\boldsymbol{F}}_{3+}\hat{\boldsymbol{F}}_{2+} + \hat{\boldsymbol{F}}_{3-}\hat{\boldsymbol{F}}_{1+}\right) \tag{16}$$

$$\hat{\boldsymbol{S}} = e^{\hat{\boldsymbol{\gamma}}_{\mathrm{DM}}\mathscr{L}}\left(\hat{\boldsymbol{F}}_{4+}\hat{\boldsymbol{F}}_{1-} + \hat{\boldsymbol{F}}_{4-}\hat{\boldsymbol{F}}_{2-}\right)$$
$$+ e^{-\hat{\boldsymbol{\gamma}}_{\mathrm{DM}}\mathscr{L}}\left(\hat{\boldsymbol{F}}_{4+}\hat{\boldsymbol{F}}_{2+} + \hat{\boldsymbol{F}}_{4-}\hat{\boldsymbol{F}}_{1+}\right) \tag{17}$$

where $\hat{\boldsymbol{\gamma}}_{\mathrm{DM}}$ is a diagonal matrix collecting all DMs propagation constants, so that $e^{\pm\hat{\boldsymbol{\gamma}}_{\mathrm{DM}}}$ is a diagonal matrix of exponential terms. Finally, the terms $\hat{\boldsymbol{F}}_{(1-4)\pm}$ are defined as

$$\hat{\boldsymbol{F}}_{1\pm} = \pm\left(\hat{\boldsymbol{\gamma}}_{\mathrm{DM}} + \hat{\gamma}_{\mathrm{CM}}\right)^{-1}\left(e^{\pm(\hat{\boldsymbol{\gamma}}_{\mathrm{DM}} + \hat{\gamma}_{\mathrm{CM}})\mathscr{L}} - \boldsymbol{1}\right) \tag{18}$$

$$\hat{\boldsymbol{F}}_{2\pm} = \left(\pm\left(\hat{\boldsymbol{\gamma}}_{\mathrm{DM}} - \hat{\gamma}_{\mathrm{CM}}\right)\right)^{-1}\left(e^{\pm(\hat{\boldsymbol{\gamma}}_{\mathrm{DM}} - \hat{\gamma}_{\mathrm{CM}})\mathscr{L}} - \boldsymbol{1}\right) \tag{19}$$

$$\hat{\boldsymbol{F}}_{3\pm} = e^{\pm\hat{\gamma}_{\mathrm{CM}}\mathscr{L}}\left(\pm\hat{V}_{\mathrm{CM}}(\mathscr{L})/\hat{Z}_\mathrm{C}^{\mathrm{CM}} + \hat{I}_{\mathrm{CM}}(\mathscr{L})\right) \tag{20}$$

$$\hat{\boldsymbol{F}}_{4\pm} = e^{\pm\hat{\gamma}_{\mathrm{CM}}\mathscr{L}}\left(\hat{V}_{\mathrm{CM}}(\mathscr{L}) \pm \hat{Z}_\mathrm{C}^{\mathrm{CM}}\hat{I}_{\mathrm{CM}}(\mathscr{L})\right) \tag{21}$$

where $\hat{\gamma}_{\mathrm{CM}}$ and $\hat{Z}_\mathrm{C}^{\mathrm{CM}}$ are scalar values representing the propagation constant and the characteristic impedance of the equivalent CM TL, and $\boldsymbol{1}$ is a $(N-1) \times (N-1)$ unitary matrix.
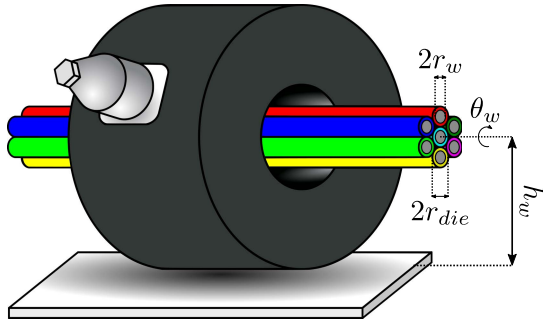
Fig. 4.   7-conductor transmission line clamped by a BCI probe.

III. VALIDATION

In this section, the proposed method is validated versus the model described in [15]. Namely, physical terminal voltages are computed via the method proposed in [15] and, then, converted into modal quantities $\hat{V}_m$ and $\hat{I}_m$ to allow a comparison with the two step-procedure here proposed. To this purpose, the seven-conductor test setup shown in Fig. 4 is considered. All wires in the bundle have the following geometrical characteristics: conductor radius $r_w = 0.4\,\mathrm{mm}$, dielectric jacket radius $r_{die} = 0.8\,\mathrm{mm}$, relative permittivity of the dielectric jacket $\varepsilon_r = 2$, center-to-center wire separation $s = 2.75\,\mathrm{mm}$, height of the cable harness (to the center wire) above ground of the bundle axis $h_w = 47.5\,\mathrm{mm}$, and the bundle rotation angle $\theta_w = 0$. According to the standard [2], the bundle length is $L_{line} = 2\,\mathrm{m}$ and the BCI probe is clamped at $150\,\mathrm{mm}$ from the EUT. The BCI probe model is based on probe FCC-F130 A, as in [15]. It can be noted that [15] is an extension of [13]: therefore, this model also works if twisted wire pairs are included in the bundle, as long as their p.u.l. parameters are properly estimated. Each wire of the bundle is terminated with $50\,\Omega$ impedance. Examples of the obtained results are shown in Fig. 5. Namely, they depict the CM [see Fig. 5(a)], DM1 [see Fig. 5(b)], and DM4 [see Fig. 5(c)] voltages. Similar accuracy is obtained for the other modal voltages. On the whole, a satisfactory agreement is achieved. Specifically, below $20\,\mathrm{MHz}$, the magnitude of CM and DM4 voltages shows discrepancies lower than $1\,\mathrm{dB}$, whereas the absolute value of the DM1 voltage has a maximum deviation of around $1.3\,\mathrm{dB}$ in the same frequency range. For higher frequencies, the observed deviations slightly increase due to small phase discrepancies at the resonant frequencies. Fig. 5(a) proves that the CM is not affected appreciably by the backinteraction from the DMs, thus confirming the effectiveness of the weak-coupling assumption. Conversely, the other modes are more affected by this approximation. In particular, this simplification leads to some mismatches in the modal terminal voltage with the lowest magnitude, i.e., DM1. Fig. 5(b) shows some differences in both the real and imaginary parts starting from low frequency, while the deviation in the magnitude of $\hat{V}_{EUT}^{DM1}$ is quite low up to about $50\,\mathrm{MHz}$. Prediction accuracy significantly improves for the other modes, which are all greater in magnitude than DM1. Indeed, Fig. 5(c) shows that the predictions of the DM4 provided by the two models essentially overlap in the entire
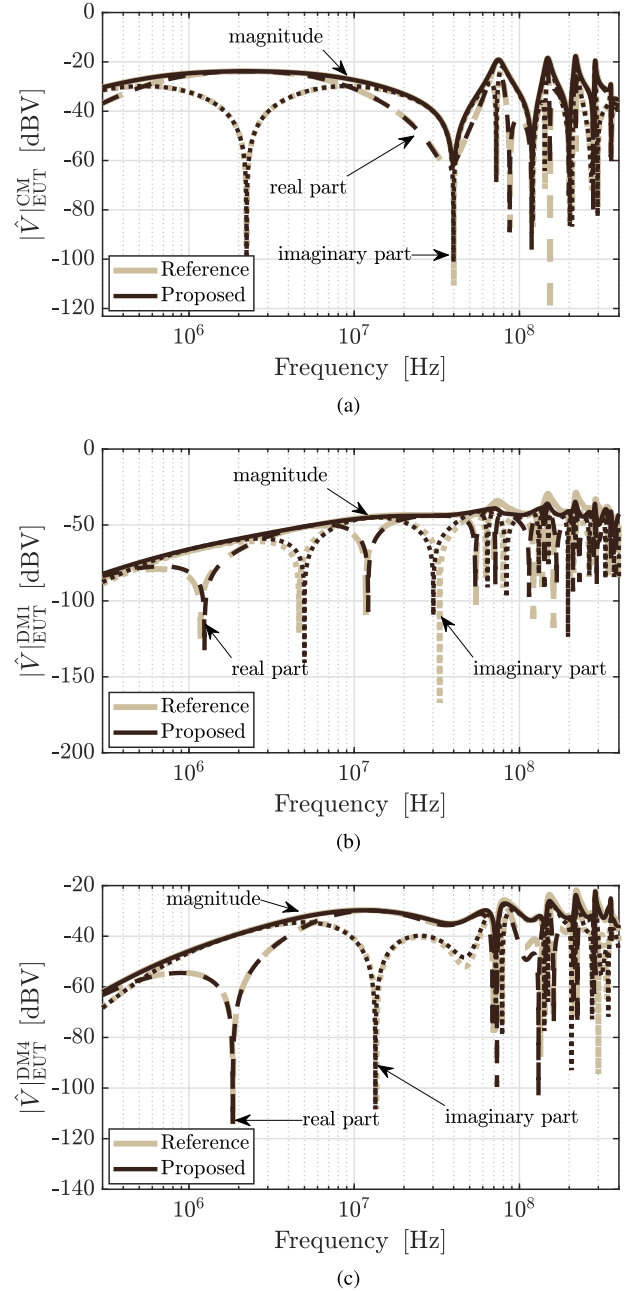

(a)

(b)

(c)

Fig. 5.   Comparison between the predicted (a) CM, (b) DM1, and (c) DM4 voltages determined at the EUT side of the setup resulting from the complete model (brown curves) and the two-step procedure (black curves). Solid, dashed, and dotted lines represent the magnitude, real, and imaginary parts, respectively.

frequency range of interest, with small discrepancies in the real and imaginary parts above $60\,\mathrm{MHz}$.

Once modal voltages are known, they can be transformed into phase voltages by reversing (3) and (4). It is worth noting that good accuracy in the prediction of phases quantities is achieved even if CM components are considered only. Indeed, there may be scenarios in which there is no interest in predicting DM quantities and, therefore, the problem simplifies from a N-conductor down to a single-conductor one. In this way, a relevant
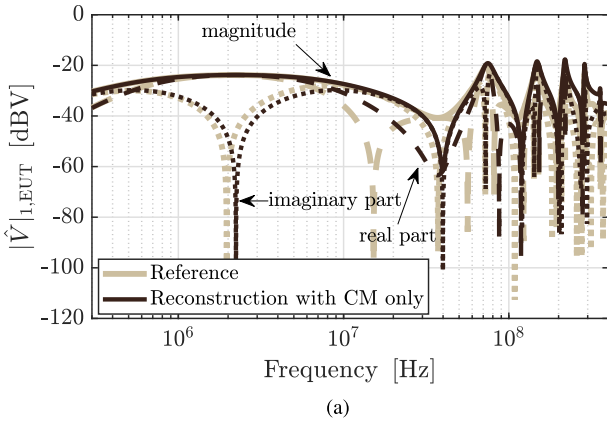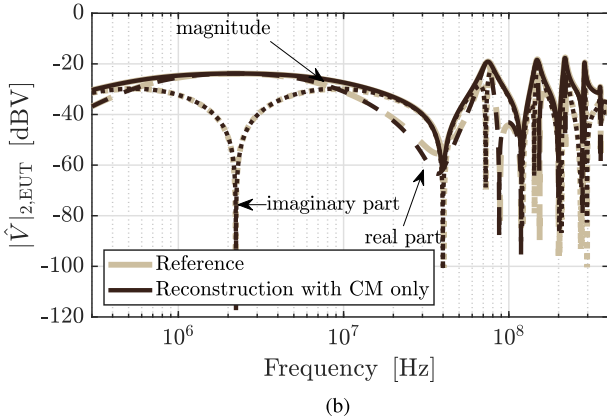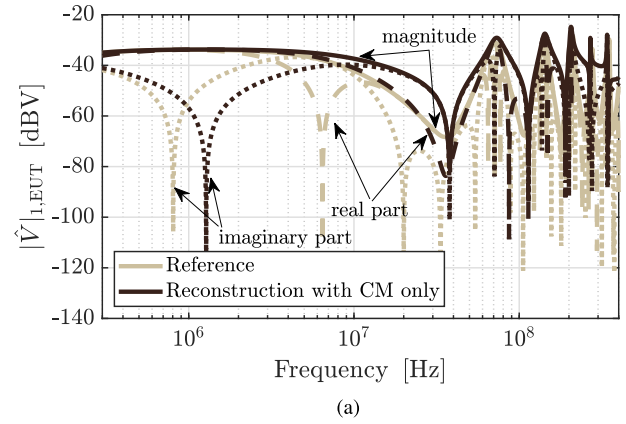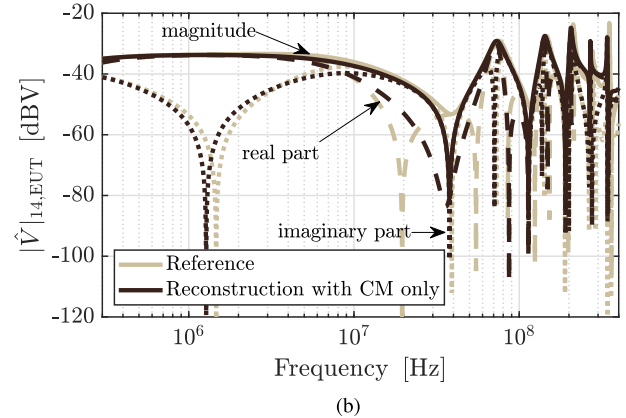
Fig. 6. Comparisons between the phase voltages of the wires placed at (a) the center and (b) the top of a seven-conductor bundle reconstructed starting from the complete model (brown lines) and CM prediction only (black lines). Solid lines stand for absolute values of the voltages, dashed ones for the real parts, and dotted lines for the imaginary parts.

Fig. 7. Comparison between the phase voltages of the wires placed (a) at the center and (b) in the second shell of conductors of a 28-wire bundle reconstructed starting from the complete model (brown lines) and CM prediction only (black lines). Solid lines stand for absolute values of the voltages, dashed lines for the real parts, and dotted lines for the imaginary parts.

amount of computational time can be saved with respect to the complete procedure. This approximation is justified once again by the CM nature of the injection probe. Indeed, this simplified approach leads to compute equal voltages and currents on each conductor of the bundle, whereas, in the reality, the presence of DM components introduces differences among the wires. Thus, a CM analysis can be run to obtain an indication on the order of magnitude of the RF injection on each wire of the bundle through a quick simulation. Fig. 6(a) shows the comparison between the phase voltage at the EUT terminations of the central wire of a seven-conductor bundle computed with the complete model versus the same voltage reconstructed by retaining the CM only. The differences observed in this plot represent a worst case, since other terminal phase voltages show a better agreement, as shown in Fig. 6(b). Indeed, the reconstructions of the magnitude of V_1 and V_2 show maximum deviations with respect to the reference model of about $1\,\mathrm{dB}$ and $0.2\,\mathrm{dB}$ below $20\,\mathrm{MHz}$, respectively. The mismatch at high frequency range is slightly larger due to small phase discrepancies at the resonant frequencies.

In principle, the proposed method can be applied to wire bundles with an arbitrary number of conductors, as reported in Section II. However, in bundles with a large number of

shells, degradation of accuracy can be observed, in particular in the prediction of voltages for the innermost wire. Specifically, the observed discrepancies start to be nonnegligible if more than three conductor shells are considered (i.e., if $N \geq 28$). Nevertheless, the predictions of terminal voltages in the majority of the wires remain accurate. This limitation is a consequence of the assumption of weak coupling between CM and DMs required by the proposed method. To provide an example, a 28-wire bundle is considered. The bundle has the cross section shown in Fig. 1, but with an additional external shell involving other equally spaced nine conductors. For this bundle, Fig. 7 shows the comparison between voltages predicted at the terminations of (a) the innermost wire and (b) one of the conductors belonging to the second shell (i.e., the one at the bottom of the shell in this example).

IV. WORST/BEST CASE SCENARIOS

In this section, the proposed deterministic method is employed and adapted to speed up the analysis of worst/best case scenarios of BCI injection tests. As discussed before, the proposed model is able to decouple the DM and CM quantities and, therefore, it

can be naturally divided into two steps: CM and DM analyses. This feature is exactly in line with the BCI injection feature. Indeed, a BCI probe is a CM injection tool and most of its information/energy is in the CM domain. Therefore, by analyzing the CM circuit only, which is the first step of the proposed method, one can get the majority of the information regarding the injected noise. Furthermore, this decoupling feature makes it possible to split the variables into those related to CM and DM. Thanks to the aforesaid advantages, the adapted modal-domain analysis can significantly improve the computational efficiency of the worst/best case analysis of BCI setups.

A. Probabilistic–Possibilistic Analysis

In order to achieve boundaries to the maximum and minimum CM and DM noise induced by BCI at the input of the units under tests, statistical techniques should be employed. For example, uncertainty effects can be characterized by assuming that geometrical or electrical parameters of BCI setups follow suitable probability distribution functions with evaluable mean and variance. In other words, these parameters can be treated as RVs and statistical analysis can be performed using probabilistic methods, such as the Monte Carlo (MC) analysis. This is the typical approach used to evaluate the effect of the tolerances of the manufacturing process and of repeated measurements as well. However, this pure probabilistic framework is not suited for all parameters in BCI setups. An example is the value of CM impedance of the terminal units. Rather than assuming that it follows a specific distribution, which is almost impossible to identify correctly, it is more realistic to recognize that the uncertainty on the CM impedance at cable terminations stems from an inherent lack of knowledge (epistemic uncertainty) [29]. Indeed, the CM impedance is here considered as the result of modal transformation of the load impedance matrix of the harness whose entries are strongly influenced by unknown parasitics. In most cases, there is no possibility to measure this parameter in practice and its magnitude is typically dependent on the specific application. Therefore, its value should be estimated somehow in a range of admissible values. To deal with epistemic uncertainty, possibility theory is exploited to define suitable variables known as fuzzy variables (FVs) [23], [30]. Detailed discussions regarding possibility theory and how possibility and probability theories can be combined for prediction purposes are reported in [26], [31], and [32]. Indeed, to deal with statistical analysis of problems involving both random and epistemic variables, hybrid probabilistic–possibilistic algorithms are available in the literature [24], [25]. These hybrid techniques are able to retain the uncertainty nature of RVs and FVs, and, recently, they have been introduced also for EMC assessments [33], [34]. To this end, statistical methods (such as MC, polynomial chaos expansion (PCE) [35], [36], [37], etc.) and optimization techniques (grid search (GS), Bayesian optimization (BO) [38], etc.) are usually employed and in combination with the hybrid probabilistic–possibilistic algorithms for the analyses of RVs and FVs, respectively. In this work, it is assumed that BCI setups involve both RVs and FVs, and the methodology presented in [34] is adopted to estimate worst- and best-case scenarios
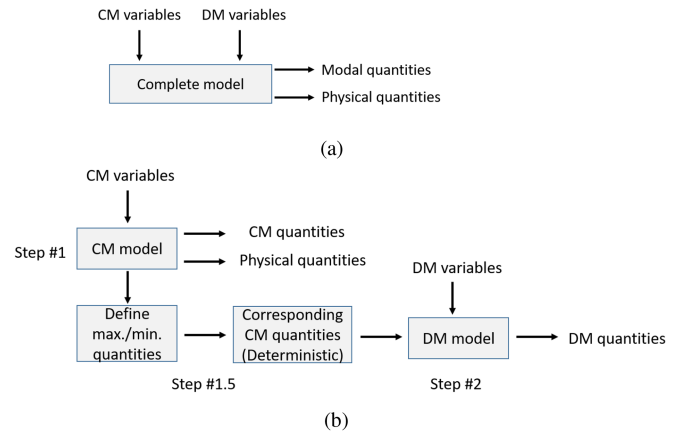

Fig. 8. Flowcharts illustrating the solution steps according to: (a) the reference method, (b) the proposed two-step procedure for worst- and best-case predictions.

in BCI testing. In particular, a combination of GS and PCE is chosen for this goal. The only difference with respect to [34] is that GS is used rather than BO, given its ease of implementation and integration with the proposed two-steps modeling approach.

Let us assume that the quantity of interest in one BCI test, for example V_{CM}, depends on a set of RVs ξ and FVs η. The methodology described in [34] allows one to estimate the boundaries delimiting, where the cumulative distribution function of the quantity of interest lies, by using only a limited number of samples (ξ, η). The obtained boundaries define worst- and best-case scenarios for the BCI test setup under analysis. Section IV-B describes how to efficiently combine the proposed two-steps approach with the methodology [34].

B. Proposed Worst/Best-Case Prediction Model

Without loss of generality, a BCI setup with N-wire bundle involving M CM-related and K DM-related variables is considered as the general structure under analysis. It is assumed that I and J (ξ, η) samples are required for CM- and DM-related variables, respectively.

The approach that will be considered as reference is to directly estimate the physical quantities (i.e., voltages and currents) at each frequency, for example, via the model [15], and based on these results evaluate the corresponding CM and DM quantities [see: Fig. 8(a)]. Then, the methodology [34] can be adopted to estimate worst- and best-case scenarios. This requires to solve $M^I \times K^J$ N-conductor problems.

Alternatively, based on the method proposed in Section II, a two-step method to predict worst/best-case scenarios is introduced. The principle diagram of the method is shown in Fig. 8(b). The first step is to address the CM equivalent circuit (see: Fig. 3(a)) and CM-related variables. To this end, the methodology presented in [34] is adopted based on the output of the CM solver only. Information on physical quantities (e.g., voltages V_1, $V_2, \ldots, V_N$) can be also obtained by employing modal transformations assuming that all DM quantities are null. Although in this step the problem involves only one equivalent conductor, it

will be shown in the following that CM analysis (step #1) is enough for accurate prediction of boundaries for both CM and physical quantities. However, in order to correctly predict DM quantities, the CM should be propagated into the DMs circuits. To this end, it is assumed that the maximum and minimum CM currents at the EUT side (and related settings) determine the highest and lowest levels of CM quantities accounting for mode conversion. Therefore, the corresponding CM complex values (such as $\hat{V}_R^{CM}(\mathscr{L})$ and $\hat{I}_R^{CM}(\mathscr{L})$ in (6)) linked to the aforesaid two cases are used as the *deterministic* inputs for the DM analysis. This is indicated as step #1.5 in Fig. 8(b). In Step #2, the statistical issues involving DM equivalent circuit (see Fig. 3(b)) and DM-related variable are solved via the method [34] based on the output of the DM solver. To sum up, the key idea of this method is to use the information obtained from the CM analysis (Step #1) to simplify the problem. In this way, the problems to be solved become M^I *one*-conductor problems (for CM and physical quantities) and $2 K^J N\text{-}1$-conductor problems (for DM quantities).

C. Numerical Examples

To validate the proposed approach, 7- and 19-wire bundles (with cross section as shown in Fig. 1) clamped by a BCI probe FCC-F130 A are considered as application examples.

Based on the aforesaid analysis and without loss of generality, RVs and FVs are assigned as follows. A preliminary investigation based on parametric analysis allowed identifying variables, which mostly influence the distribution of the induced CM and DM quantities. Among them, geometrical characteristics of the bundle, such as h_w, r_w, and θ_w are found to be responsible to appreciable variations in the induced DM quantities, since they do not significantly influence the CM. Although nominal values for these parameters are available, their actual values can differ from the nominal ones due to uncertainty in the realization of the test setup. Gaussian distributions are ideal for representing such a random uncertainty. Therefore, h_w, r_w, and θ_w are treated as RVs normally distributed around the nominal values $70\,\mathrm{mm}$, $0.4\,\mathrm{mm}$, and 0 with $10\,\mathrm{mm}$, $0.05\,\mathrm{mm}$, and $6°$ standard deviation, respectively. Conversely, among the parameters influencing the CM (and therefore also the DM through mode conversion), CM terminal impedances were identified as critical parameters. Such impedances strictly depend on the terminal units as well as on their installation. Hence, information on their values is usually not available, unless preliminary measurement can be run. Such a lack of information can be better represented using the concept of epistemic uncertainty and exploiting possibility theory, rather than assigning an (arbitrary) probability distribution to characterize the variability of terminal impedances in the BCI setup under study. Specifically, a rectangular possibility distribution $[0\,1000]\ \Omega$ is chosen to represent a plausible variability range of the CM impedance at left (R_{CML}) and right (R_{CMR}) terminals. A rectangular possibility distribution indicates that R_{CML} and R_{CMR} impedances can assume all values in the interval $[0\,1000]\ \Omega$ (possible values), whereas values outside the specified interval are impossible. However, no assumption is made on the *likelihood* of the values in such

TABLE I
COMPUTATIONAL TIME: SEVEN-CONDUCTOR BCI SETUP

		Reference	Proposed
CM	Sim. time	3654 s	163 s
	Speed-up		×22.4
CM+DM	Sim. time	3654 s	213 s
	Speed-up		×17.2
Physical-domain	Sim. time	3602 s	166 s
	Speed-up		×21.7

TABLE II
COMPUTATIONAL TIME: NINETEEN-CONDUCTOR BCI SETUP

		Reference	Proposed
CM	Sim. time	8669 s	246 s
	Speed-up		×35.2
CM+DM	Sim. time	8669 s	367 s
	Speed-up		×23.6
Physical-domain	Sim. time	8662 s	246 s
	Speed-up		×35.2

interval [31], [32]. This approach is more suitable to perform our worst/best-case analysis than adopting probability theory, since estimating the correct probability distribution to accurately describe the variability of CM terminal impedances is difficult, in practice, and would require to perform measurements on a large number of different BCI test setup. Hence, we will hereafter consider the impedances R_{CML} and R_{CMR} as variables for the solution of the CM circuit. Conversely, geometrical variables will be considered just for the solution of the DM circuit, as they were found to scarcely influence the CM.

In this worst/best-case analysis, the method [34] based on GS and PCE is employed to deal with FVs and RVs, respectively, as mentioned in Section IV-A. Specifically, 20 linear-spaced samples are considered for each FV (i.e., R_{CML} and R_{CMR}) when GS is used for the identification of extreme values (i.e., minima and maxima), while a second-order PCE method [34], [39] based on [40] is applied for micromodeling of RV samples. Note that the minimum/maximum quantities defined in Step #1.5 are CM currents at the EUT side in the proposed two-step method. Figs. 9 and 10 present the predicted worst and best cases for V_{CM}, V_{DM1}, V_{DM4} (seven-wire)/V_{DM14} (nineteen-wire), and V_1, showing a good agreement between the reference method and the proposed one. Specifically, except for some small values at low frequencies, the differences between the proposed and reference results are within $2\,\mathrm{dB}$ up to $20\,\mathrm{MHz}$. After $20\,\mathrm{MHz}$, the accuracy decreases (especially at the resonance frequencies), yet the predictions can still show reliable upper bounds in the high frequency range. Similar accuracy is achieved also for the other lines/modes, but they are not reported here for the sake of brevity. Worst-case predictions exhibit higher accuracy, since some quite low (and low probability) values may occur below $20\,\mathrm{MHz}$ or at the resonant frequencies.
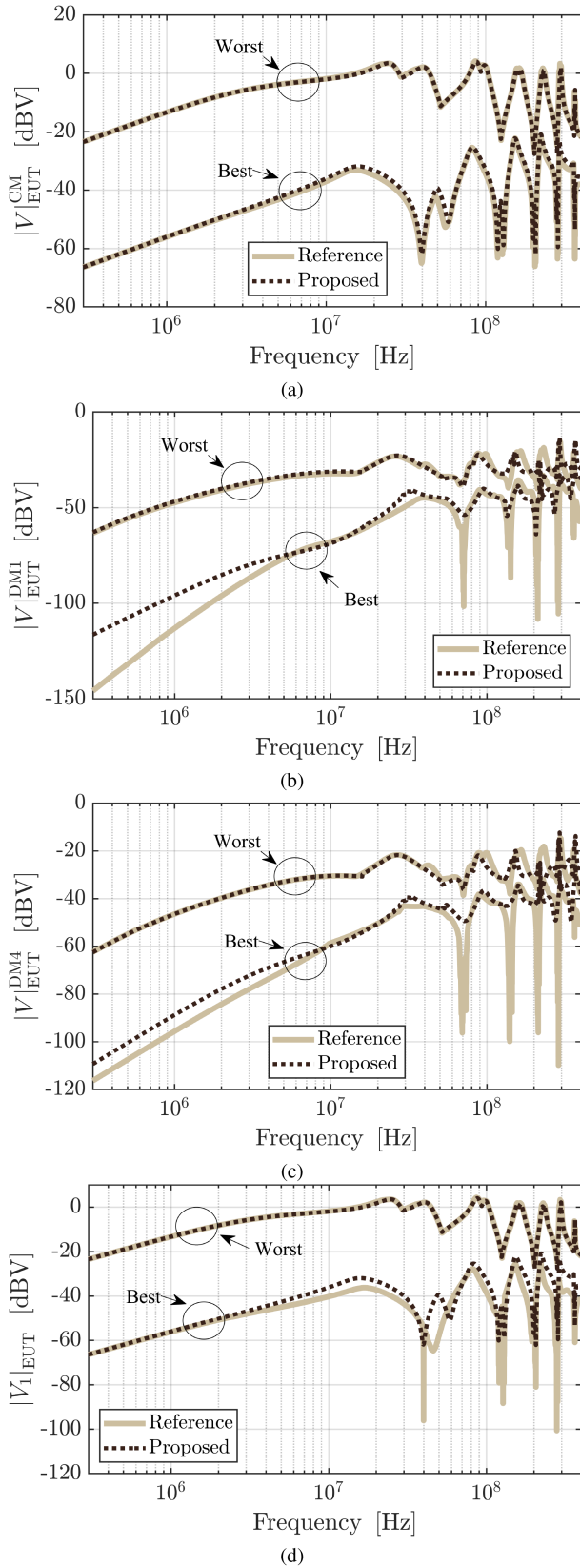
Fig. 9.   Prediction of worst and best cases of (a) V_{CM}, (b) V_{DM1}, (c) V_{DM4}, and (d) V_1 computed at EUT side of the seven-wire setup based on the reference method and the proposed methods.
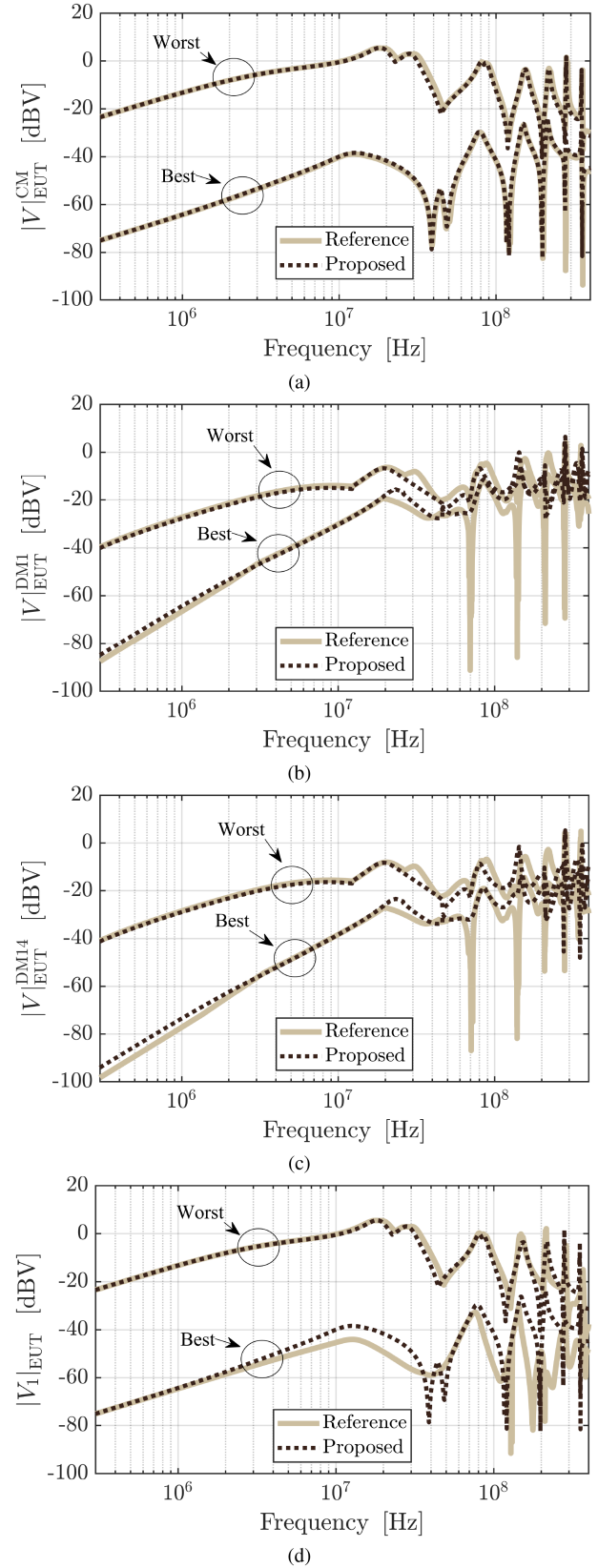
Fig. 10.   Prediction of worst and best cases of (a) V_{CM}, (b) V_{DM1}, (c) V_{DM14}, and (d) V_1 computed at EUT side of the nineteen-wire setup based on the reference method and the proposed methods.

D. Computational Efficiency

In Tables I and II, the computational time required by the proposed method to predict modal and physical quantities is compared versus the time required by the reference method. The impacts of statistic/optimization methods themselves are excluded since the same techniques (i.e., GS and PCE) are considered for both reference and proposed methods. In order to build accurate PCE models as a function of the RVs, ten samples of the random parameters are used. To this end, AN-SYS Maxwell is employed to obtain the corresponding p.u.l. parameters of those samples (involving the stretches of MTLs with and without the BCI probes), which require 570 s and 881 s for seven-wire and nineteen-wire problems, respectively. These costs are identical for both reference and proposed methods, since they are based on the methodology described in [34] to quantify the uncertainty.

Conversely, the advantages of the proposed method are significant in terms of reduction of the number and size of the problems to be solved, leading to a significant speed-up of the solution process as shown in Tables I and II. Indeed, in the considered examples GS and PCE require 400 (20^2) and 10 samples, respectively. This means that (by employing the reference method), 4000 seven-/nineteen-wire problems need to be solved. However, in the proposed two-step approach, if the target is the prediction of CM and physical quantities, the proposed method requires the solution of 400 one-conductor problems. When DM prediction is the target, additional 10 $N-1$ wire problems need to be solved for the worst and for the best-case analysis, for a total of 20 six-wire problems for the seven-wire configuration and 20 eighteen-wire problems for the nineteen-wire configuration. The number and size of problems that need to be solved in the proposed methods is much smaller than in the traditional method. Therefore, the proposed method is significantly more efficient than the reference one.

V. CONCLUSION

This work has addressed the modeling of BCI test setups involving wiring harnesses. Particularly, a two-step procedure has been developed, which allows computationally effective prediction of the maximum and minimum levels of noise induced at the terminal sections, despite some parameters of the test setup are affected by uncertainty and/or unknown to the user. To this end, CM and DM quantities have been introduced by a suitable modal transformation, and a deterministic model has been developed, which foresees the solution of the CM (dominant mode) equivalent circuit as the first step. The predicted CM quantities are then used as input quantities for the prediction of the (N−1) DMs, by solution of an equivalent modal circuit involving (N-1) equivalent wires as well as controlled voltage and current sources accounting for CM-to-DM conversion. The advantage of this model stems from the fact that the BCI probe is included in the CM equivalent circuit only, which makes easier correlating the results obtained by the model with the calibration data and the requirements foreseen by the standards (which refer to a single-wire interconnection). Preliminary sensitivity

analyses carried out by this model led to the identification of a set of parameters mainly influencing CM (DMs) quantities, which allowed applying the proposed two-step approach to investigate the sensitivity of the induced noise quantities to possible variation of setup parameters.

More specifically, this two-step procedure has been exploited to develop a novel hybrid probabilistic–possibilistic framework for the evaluation of the maximum/minimum noise injected by BCI into the terminal networks. The proposed two-step analysis foresees uncertainty propagation from the CM to the DMs, and it proved to be more efficient in terms of computational time than the reference procedure exploiting physical instead of modal quantities. Namely, the proposed procedure requires the solution of a fewer number of wire problems. For instance, the analysis of setups involving seven and nineteen wire bundles allowed appreciating a speed-up ranging from $\times 17$ up to $\times 35$ with respect to the reference solution.

REFERENCES

[1] *Environmental Conditions and Test Procedures for Airborne Equipment, Section 20: Radio Frequency Susceptibility (Radiated and Conducted)*, RTCA DO-160G ed., 2014.

[2] *Road Vehicles - Component Test Methods for Electrical Disturbances from Narrowband Radiated Eletcromagnetic Energy - Part 4: Harness Excitation Methods*, ISO 11452-4 ed., 2011.

[3] *Electromagnetic Compatibility (EMC)—Part 4: Testing and Measurement Techniques—Section 6: Immunity to Conducted Disturbances*, IEC 61000-4-6 ed., 2017.

[4] *Requirements for the Control of Electromagnetic Interference Characteristics of Subsystems and Equipment*, MIL-STD-461G ed., 2015.

[5] M. Cuvelier, J. Rioult, M. Klingler, and S. Ficheux, "Double bulk current injection: A new harness setup to correlate immunity test methods," in *Proc. Int. Symp. Electromagn. Compat.*, 2003, pp. 225–228.

[6] X. Lu, G. Wei, X. Pan, X. Zhou, and L. Fan, "A pulsed differential-mode current injection method for electromagnetic pulse field susceptibility assessment of antenna systems," *IEEE Trans. Electromagn. Compat.*, vol. 57, no. 6, pp. 1435–1446, Dec. 2015.

[7] K. Murano, M. Hoshino, Y. Kami, F. Xiao, and M. Tayarani, "Modelling of transmission line loaded with BCI probe using circuit concept approach," in *Proc. IEEE Int. Symp. Electromagn. Compat.*, 2017, pp. 1–4.

[8] F. Lafon, Y. Belakhouy, and F. De Daran, "Injection probe modeling for bulk current injection test on multiconductor transmission lines," presented at the IEEE Symp. Embedded EMC, Rouen, France, Jan. 2007.

[9] S. Miropolsky, S. Frei, and J. Frensch, "Modeling of bulk current injection (BCI) setups for virtual automotive IC tests," in *Proc. IEEE Int. Symp. Electromagn. Compat.*, 2010, Art. no. 2.

[10] F. Grassi, F. Marliani, and S. A. Pignari, "Circuit modeling of injection probes for bulk current injection," *IEEE Trans. Electromagn. Compat.*, vol. 49, no. 3, pp. 563–576, Aug. 2007.

[11] I. Oganezova, X. Bunlon, A. Gheonjian, I. Chahine, B. Khvitia, and R. Jobava, "A new and easy approach to create BCI models," in *Proc. Int. Symp. Electromagn. Compat.*, 2014, pp. 91–96.

[12] X. Liu et al., "Behavioral modeling of complex magnetic permeability with high-order Debye model and equivalent circuits," *IEEE Trans. Electromagn. Compat.*, vol. 63, no. 3, pp. 730–738, Jun. 2021.

[13] F. Grassi and S. A. Pignari, "Bulk current injection in twisted wire pairs with not perfectly balanced terminations," *IEEE Trans. Electromagn. Compat.*, vol. 55, no. 6, pp. 1293–1301, Dec. 2013.

[14] P. DeRoy and S. Piper, "Full-wave modeling of bulk current injection probe coupling to multi-conductor cable bundles," in *Proc. Int. Symp. Electromagn. Compat.*, 2016, pp. 770–774.

[15] N. Toscani, F. Grassi, G. Spadacini, and S. A. Pignari, "Circuit and electromagnetic modeling of bulk current injection test setups involving complex wiring harnesses," *IEEE Trans. Electromagn. Compat.*, vol. 60, no. 6, pp. 1752–1760, Dec. 2018.

[16] A. M. Sánchez, A. Pérez, J. R. Regué, M. Ribó, P. Rodríguez-Cepeda, and F. J. Pajares, "A modal model of common-mode chokes for conducted interference prediction," *IEEE Trans. Electromagn. Compat.*, vol. 52, no. 3, pp. 749–752, Aug. 2010.

[17] X. Wu, F. Grassi, P. Manfredi, D. Vande Ginste, and S. A. Pignari, "Compensating mode conversion due to bend discontinuities through intentional trace asymmetry," *IEEE Trans. Electromagn. Compat.*, vol. 62, no. 2, pp. 617–621, Apr. 2020.

[18] A. Sugiura and Y. Kami, "Generation and propagation of common-mode currents in a balanced two-conductor line," *IEEE Trans. Electromagn. Compat.*, vol. 54, no. 2, pp. 466–473, Apr. 2012.

[19] F. Grassi, X. Wu, Y. Yang, G. Spadacini, and S. A. Pignari, "Modeling of imbalance in differential lines targeted to spice simulation," *Prog. Electromagn. Res. B*, vol. 62, pp. 225–239, 2015.

[20] K. Sejima, Y. Toyota, K. Iokibe, L. R. Koga, and T. Watanabe, "Experimental model validation of mode-conversion sources introduced to modal equivalent circuit," in *Proc. Int. Symp. Electromagn. Compat.*, 2012, pp. 492–497.

[21] C. Su and T. H. Hubing, "Imbalance difference model for common-mode radiation from printed circuit boards," *IEEE Trans. Electromagn. Compat.*, vol. 53, no. 1, pp. 150–156, Feb. 2011.

[22] F. Grassi, Y. Yang, X. Wu, G. Spadacini, and S. A. Pignari, "On mode conversion in geometrically unbalanced differential lines and its analogy with crosstalk," *IEEE Trans. Electromagn. Compat.*, vol. 57, no. 2, pp. 283–291, Apr. 2015.

[23] L. A. Zadeh, "Fuzzy sets as a basis for a theory of possibility," *Fuzzy Sets Syst.*, vol. 1, pp. 3–28, 1978.

[24] C. Baudrit, D. Guyonnet, and D. Dubois, "Post-processing the hybrid method for addressing uncertainty in risk assessment," *J. Environ. Eng.*, vol. 131, no. 2, pp. 1750–1754, Dec. 2005.

[25] C. Baudrit, D. Dubois, and D. Guyonnet, "Joint propagation and exploitation of probabilistic and possibilistic information in risk assessment," *IEEE Trans. Fuzzy Syst.*, vol. 14, no. 5, pp. 593–608, Oct. 2006.

[26] P. Baraldi, I. C. Popescu, and E. Zio, "Predicting the time to failure of a randomly degrading component by a hybrid Monte Carlo and possibilistic method," in *Proc. Int. Conf. Prognostics Health Manage.*, 2008, pp. 1–8.

[27] D. Bockelman and W. Eisenstadt, "Combined differential and common-mode scattering parameters: Theory and simulation," *IEEE Trans. Microw. Theory Techn.*, vol. 43, no. 7, pp. 1530–1539, Jul. 1995.

[28] C. R. Paul, *Introduction to Electromagnetic Compatibility*. Hoboken, NJ, USA: Wiley, 2006.

[29] S. Salicone, *Measurement Uncertainty: An Approach via the Mathematical Theory of Evidence*. Berlin, Germany: Springer, 2007.

[30] G. Shafer, *A Mathematical Theory of Evidence*, vol. 42. Princeton, NJ, USA: Princeton Univ. Press, 1976.

[31] D. Dubois and H. Prade, "When upper probabilities are possibility measures," *Fuzzy Sets Syst.*, vol. 49, no. 1, pp. 65–74, Jul. 1992.

[32] A. Ferrero and S. Salicone, "The random-fuzzy variables: A new approach for the expression of uncertainty in measurement," in *Proc. 20th IEEE Instrum. Technol. Conf.*, 2003, pp. 1502–1507.

[33] L. Badini, N. Toscani, G. Spadacini, F. Grassi, and S. A. Pignari, "A possibilistic approach to radiated susceptibility of twisted-wire pairs," in *Proc. IEEE Int. Symp. Electromagn. Compat. Signal/Power Integrity*, 2017, pp. 96–101.

[34] S. De Ridder, D. Spina, N. Toscani, F. Grassi, D. Vande Ginste, and T. Dhaene, "Machine-learning-based hybrid random-fuzzy uncertainty quantification for EMC and SI assessment," *IEEE Trans. Electromagn. Compat.*, vol. 62, no. 6, pp. 2538–2546, Dec. 2020.

[35] P. Manfredi, D. Vande Ginste, I. S. Stievano, D. De Zutter, and F. G. Canavero, "Stochastic transmission line analysis via polynomial chaos methods: An overview," *IEEE Electromagn. Compat. Mag.*, vol. 6, no. 3, pp. 77–84, Third Quarter 2017.

[36] A. Kaintura, T. Dhaene, and D. Spina, "Review of polynomial chaos-based methods for uncertainty quantification in modern integrated circuits," *Electronics*, vol. 7, no. 3, 2018, Art. no. 30. [Online]. Available: https://www.mdpi.com/2079-9292/7/3/30

[37] Y. Ye, D. Spina, P. Manfredi, D. Vande Ginste, and T. Dhaene, "A comprehensive and modular stochastic modeling framework for the variability-aware assessment of signal integrity in high-speed links," *IEEE Trans. Electromagn. Compat.*, vol. 60, no. 2, pp. 459–467, Apr. 2018.

[38] B. Shahriari, K. Swersky, Z. Wang, R. P. Adams, and N. de Freitas, "Taking the human out of the loop: A review of Bayesian optimization," *Proc. IEEE*, vol. 104, no. 1, pp. 148–175, Jan. 2016.

[39] P. Manfredi, D. Vande Ginste, D. De Zutter, and F. G. Canavero, "Generalized decoupled polynomial chaos for nonlinear circuits with many random parameters," *IEEE Microw. Wireless Compon. Lett.*, vol. 25, no. 8, pp. 505–507, Aug. 2015.

[40] Z. Zhang, T. A. El-Moselhy, I. M. Elfadel, and L. Daniel, "Stochastic testing method for transistor-level uncertainty quantification based on generalized polynomial chaos," *IEEE Trans. Comput.-Aided Des. Integr. Circuits Syst.*, vol. 32, no. 10, pp. 1533–1545, Oct. 2013.

Nicola Toscani (Member IEEE) received the B.Sc., M.Sc., and Ph.D. degrees in electrical engineering from the Politecnico di Milano, Milan, Italy, in 2013, 2015, and 2019, respectively.

He is currently working as a Postdoctoral Research Fellow with the Department of Mechanical Engineering, Politecnico di Milano. He co-founded the startup ePEBBˢ in 2021. His last research activities deal with the study and the development of recharging stations for light electric vehicles and wireless power transfer solutions. His research interests also include electromagnetic compatibility, power electronics and electrical drives.
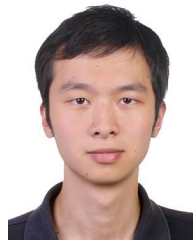
Xinglong Wu (Member, IEEE) received the double M.Sc. degrees from Xi'an Jiaotong University, Xi'an, China, and Politecnico di Milano, Milan, Italy, in 2015, and the Ph.D. degree (*summa cum laude*) from Politecnico di Milano, in 2019, all in electrical engineering.

He is currently an Assistant Professor with the Department of Electronics, Information and Bioengineering, Politecnico di Milano. In March 2017 and June 2017, he was a Visiting Scientist with the Electromagnetics Group, Department of Information Technology, Ghent University, Belgium. From 2019 to 2020, he was a Postdoctoral Research Fellow with Politecnico di Milano. His research interests include distributed parameter circuit modeling, statistical techniques for electromagnetic compatibility (EMC), experimental procedures and setups for EMC testing, and system-level EMC.

Dr. Wu received the International Union of Radio Science Young Scientist Award from the 2020 URSI General Assembly and Scientific Symposium.

Domenico Spina (Member, IEEE) received the M.S. degree (*cum laude*) in electronics engineering from the University of L'Aquila, L'Aquila, Italy, in 2010, and the joint Ph.D. degree in electrical engineering from the Ghent University, Ghent, Belgium, and the University of L'Aquila in 2014.

Since 2015, he has been a member of the Internet and Data Science Lab, Department of Information Technology, Ghent University—imec, first as Postdoctoral Researcher and currently as R&D Technical Lead. His research interests include modeling and simulation, uncertainty quantification, and machine learning for analog electronic and photonic systems.

Dries Vande Ginste (Senior Member, IEEE) received the M.S. and Ph.D. degrees in electrical engineering from Ghent University, Gent, Belgium, in 2000 and 2005, respectively.

He is currently an Associate Professor at Ghent University and imec, heading the research lab quest. In June and July 2004, he was a Visiting Scientist with the Department of Electrical and Computer Engineering, University of Illinois at Urbana-Champaign, IL, USA. From September to November 2011, he was a Visiting Professor at the EMC Group, Dipartimento di Elettronica, Politecnico di Torino, Italy. He has authored or coauthored more than 200 papers in international journals and in conference proceedings. His research interests include computational quantum mechanics and electromagnetics, electromagnetic compatibility, signal, and power integrity.

Dr. Vande Ginste was awarded the International Union of Radio Science Young Scientist Award at the 2011 URSI General Assembly and Scientific Symposium, the Best Poster Paper Award at the 2012 IEEE Electrical Design of Advanced Packaging and Systems Symposium, the Best Paper Award at the 2013 IEEE Workshop on Signal and Power Integrity, the Best Paper Award at the 2013 IEEE International Conference on Electrical Performance of Electronic Packaging and Systems, and the Best Paper Award at the 2016 IEEE Electrical Design of Advanced Packaging and Systems Symposium. He served as the Chair of the 2014 IEEE Workshop on Signal and Power Integrity. He is an Associate Editor for IEEE Transactions on Signal and Power Integrity.

Flavia Grassi (Senior Member, IEEE) received the laurea (M.Sc.) and Ph.D. degrees in electrical engineering from Politecnico di Milano, Milan, Italy, in 2002 and 2006, respectively.

She is currently a Full Professor with the Department of Electronics, Information and Bioengineering, Politecnico di Milano. From 2008 to 2009, she was with the European Space Agency (ESA), ESA/ESTEC, The Netherlands, as a Research Fellow. Her research interests include: Theoretical and experimental characterization of EM interference via lumped and distributed circuit modeling; characterization and development of measurement procedures and setups for EMC assessment of avionic, automotive, and power systems; statistical techniques, EMC and coexistence issues in power systems.

Dr. Grassi received the International Union of Radio Science Young Scientist Award in 2008, and the IEEE Young Scientist Award at the 2016 Asia-Pacific International Symposium on EMC, the IEEE EMC Society 2016 and 2021 Transactions Prize Paper Award, and the Best Symposium Paper Award at the 2015 and 2018 APEMC.